Anisotropic magnetoresistance of single-crystal $HoNi_2B_2C$ and the interplay of magnetic and superconducting order

K. D. D. Rathnayaka and D. G. Naugle
Department of Physics, Texas A&M University, College Station, Texas 77843-4242

B. K. Cho and P. C. Canfield
Ames Laboratory and Iowa State University, Ames, Iowa 50011
(Received 31 July 1995)

The in-plane resistivity and magnetization measurements as a function of the magnitude and direction of the magnetic field and the temperature are reported for single-crystal samples of the $HoNi_2B_2C$ magnetic superconductor. Features corresponding to several distinct magnetic phases and the coexistence of superconductivity with two of the magnetic phases are observed. Contrary to previous measurements for polycrystalline samples, reentrant superconductivity is not observed in the absence of a field for these samples. The measurements indicate an extremely rich interplay between superconductivity and different magnetic structures that can be influenced by field, temperature, and current. The results correlate quantitatively with and complement previous determinations of the magnetic phase diagram and qualitatively with determinations of the superconducting phases by measurements of the single-crystal magnetization and heat capacity. $HoNi_2B_2C$ is highly anisotropic, and phase diagrams for the field along the (100) and (001) directions are presented.

INTRODUCTION

A new family of layered superconductors, quaternary borocarbides, has been recently discovered.[1,2] The highest superconducting transition temperature observed in this family is 23 K for a multiphase material $YPd_5B_3C_{0.35}$.[2] The first single-phase superconducting compound to be reported[3] is $LuNi_2B_2C$ with a superconducting transition temperature of 16.6 K. The structure is tetragonal with alternating square planar layers of rare earth carbide and corrugated Ni_2B_2 sheets with a unit cell consisting of two formula units.[3] Subsequently, other superconducting rare-earth borocarbides RNi_2B_2C have been found[4] with R=Tm, Er, Ho, and Dy (Refs. 5 and 6) (T_c=11.0, 10.5, 8, and 6.2 K, respectively) as well as YNi_2B_2C with T_c=15.6 K. The transition temperatures of the compounds with magnetic rare-earth ions correlate well with the de Gennes factor, indicating that pair breaking by a localized magnetic moment may explain the variation in T_c with R.[7] A strong interplay between superconductivity and magnetic ordering is observed in the resistive transition curves of polycrystalline samples with reentrance to the normal state below T_c reported for R=Ho and in magnetic fields for R=Er and Tm.[7] Magnetic ordering occurs at T_M=1.5 K for R=Tm (Ref. 8) and 6.0 K for R=Er,[9] but there are at least two magnetic transitions (6 and 5.2 K) observed for R=Ho.[10–16] Although band structure calculations[17,18] for $LuNi_2B_2C$ suggest a high degree of isotropy in the electronic properties for this material, it is clear that there will be large anisotropies in the magnetic properties of those compounds exhibiting magnetic ordering and in the interplay of superconductivity and magnetism in the presence of a magnetic field. In previous studies of the coexistence of magnetism and superconductivity (see Fischer[19] and Bulaevskii *et al.*[20] for recent reviews) experimental limitations included very limited availability of single-crystal samples and the fact that magnetism onset only at very low temperatures. In the new rare-earth borocarbides, however, the magnetic transitions occur in an easily accessible temperature range with a variation of T_M/T_c ranging from about 0.7 for Ho to 0.15 for Tm, and single crystals have recently become available[10,21] so that the effect of magnetic anisotropy can be studied.

Of particular interest is $HoNi_2B_2C$ where complex magnetic behavior is observed to coexist with superconductivity. In zero field, three features in both the heat capacity C_P and in the magnetic susceptibility ($d\chi T/dT$) indicate magnetic phase transitions at 6.0, 5.5 and 5.2 K.[10] Single-crystal neutron scattering[12,13] indicates the onset of an oscillatory spiral magnetic state at 6 K which transforms into a commensurate antiferromagnet consisting of ferromagnetic holmium-carbide sheets with alternating directions of the magnetization near 5 K in zero field. The magnetization appears to lie in the Ho-C plane, but the preferential orientation in the plane has not been determined. Neutron scattering from polycrystalline samples[14–16] confirms the transformation to the commensurate antiferromagnetic state near 5 K, but finds that the oscillatory state appears at higher temperature (about 8 K) than the sharp onset at 6 K observed for single crystals.[12,13] The transition at 5.5 K seen in C_P and $d\chi T/dT$, however, is not readily discernible in any of the neutron-scattering experiments.

The in-plane magnetic susceptibility at low temperature for $HoNi_2B_2C$ is a factor of 50 larger than the susceptibility parallel to the c axis due to the crystal field at the Ho^{3+} site,[10,22] and, the field dependence for this series of magnetic transitions, is different for the field applied in the plane and that along the c axis or (001) direction.[11] These differences are illustrated in Fig. 1 where the locii of features in $d\chi T/dT$ taken from $M(T)$ measurements at constant H and representative of the phase transitions[10,11] are plotted for fields along the c axis and along the $a(b)$ axis. For the field applied along the c axis there is practically no field dependence for

 © 1996 The American Physical Society

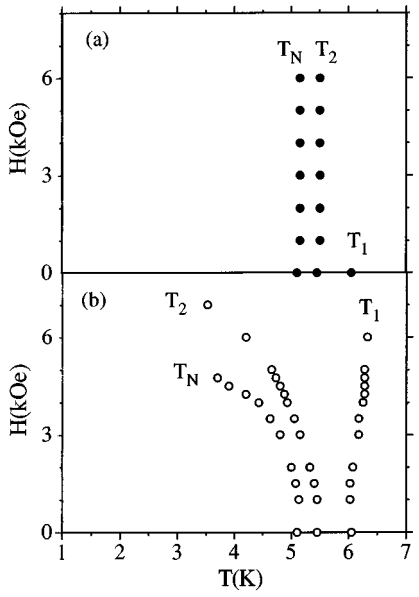

FIG. 1. Magnetic phase boundary for $HoNi_2B_2C$ with (a) the magnetic field applied along the c axis (solid circles) and (b) along the $a(b)$ axis (open circles) as indicated from magnetization measurements $M(T)$ taken at constant applied field (Refs. 10 and 11) and heat-capacity measurements in zero applied field (Ref. 10). The three phase transitions are labeled T_1, T_2, and T_N from high to low temperature.

the lower two transitions, and the higher temperature transition cannot be resolved in $d\chi T/dT$ with the field applied in this direction. For the field applied along the $a(b)$ axis all three transitions can be clearly resolved. The higher temperature transition is relatively field independent while the lower two transitions are suppressed by increasing applied field in this direction. In the absence of a field the three transitions are clearly seen in C_P features indicated by the $H_a=0$ data points[10] which are consistent with extrapolations of the locii of features in $d\chi T/dT$ to $H_a=0$. The anisotropy illustrated in this phase diagram demonstrates the importance of single-crystal samples for measurements in an applied field.

While the magnetic phase transitions can be clearly resolved via $M(T)$ measurements, $H_{c2}(T)$ can only be estimated via $M(T)$ data. This is primarily due to questions of (1) reversibility and (2) subtraction of the large paramagnetic background associated with the Ho^{3+} moments. An important question that arises naturally is how $H_{c2}(T)$ relates to the magnetic phase boundaries. In specific, there is the question of whether superconductivity stabilizes the commensurate antiferromagnetic phase. If this is the case, $H_{c2}(T)$ should coincide with the lower magnetic phase boundary. In this paper we present magnetoresistance data (as well as new magnetization data) for single-crystal samples with the goal of more fully defining the magnetic and superconducting phase boundaries of $HoNi_2B_2C$. Due to the large anisotropies associated with this material, we have measured $R(T,H)$ and $M(T,H)$ for applied fields along both the c axis and the $a(b)$ axis.

EXPERIMENT

Single crystals of $HoNi_2B_2C$ have been grown by a Ni_2B flux method.[9,21] In this method, an arc-melted and annealed button of single-phase $HoNi_2B_2C$ is placed in an alumina crucible and approximately equal mass of Ni_2B is placed beneath it. These materials are then heated in flowing argon to 1490 °C and cooled to 1200 °C at 10 °C/h, followed by furnace cooling to room temperature. Single crystals of $HoNi_2B_2C$ grow into the Ni_2B flux from the original polycrystalline button as a result of this growth schedule. The crystals can be removed from the excess Ni_2B and are platelike with either square or irregular surfaces in the ab-plane and weigh up to 500 mg.

Samples for transport measurements were ground into an approximately rectangular shape (1.4 mm×0.51 mm) from a 0.10 mm thick crystal of larger dimension. Four terminal dc resistivity measurements were carried out with 0.025 mm thick silver foils (indium soldered to obtain low contact resistance) as current leads and 0.1 mm copper wires attached to the sample using Epotek 410E epoxy as voltage leads. The low-temperature cryostat consists of an inner sample can where the sample holder assembly is located and an outer vacuum can. The sample can is partially filled with He exchange gas (50–100 torr at room temperature) for good thermal anchoring. The sample holder inside the sample can is designed so that it can be rotated by 180° about a horizontal axis to change the orientation of the sample in the field, and a Hall probe is mounted on the sample holder to measure the field as well as to orient the ab plane of the crystal with respect to the magnetic field. Most of the measurements were carried out at a sample current of 50 mA (current density of about 95 A/cm^2) employing a Keithley 181 nanovoltmeter for voltage measurements, and the sample is oriented such that the direction of the magnetic field is always normal to the current. The current dependence of the critical field was investigated at several different currents, down to 0.5 mA (0.95 A/cm^2). The temperature was controlled and ramped using a Lake Shore Cryotronics capacitance temperature controller with typical ramp rates of about 50–200 mK per min, and temperature was measured with a calibrated carbon glass thermometer. Temperature measurements were not corrected for the magnetic field dependence; however, these errors are calculated to be less than 50 mK at the highest field of 5 T used and less than 15 mK below 2 T. No correction of the field values for the demagnetization factor of the samples is included. A MacIIci based data acquisition system was used to take data and control the temperature and the magnetic field. To check that the resistance samples were representative of other single crystals, the magnetization of the oriented sample was measured with a Quantum Design SQUID Magnetometer. The orientation of that single-crystal sample was determined by x-ray diffraction, and the current was applied along the $a(b)$ axis for the resistance measurements. Magnetization measurements at fixed temperature as a function of applied field were also made on larger single-crystal samples with the same SQUID for the field applied along the a axis to help determine the details of the magnetic phase boundary.

RESULTS

The temperature dependence of the in-plane resistivity of a single-crystal $HoNi_2B_2C$ sample is shown in Fig. 2 in comparison with that of a single crystal of the nonmagnetic

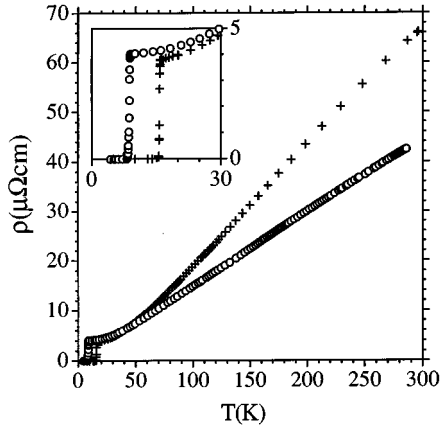

FIG. 2. Temperature dependence of the in-plane resistivity of single-crystal samples of $HoNi_2B_2C$ (open circles) and the analogous nonmagnetic compound YNi_2B_2C (crosses).

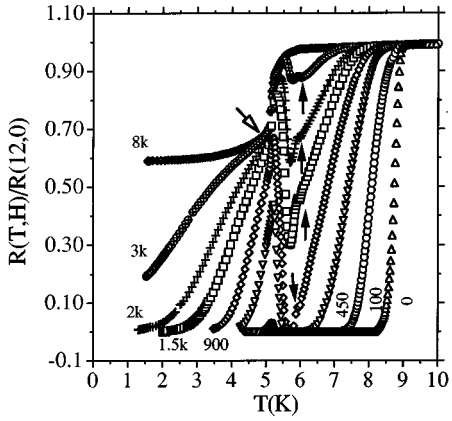

FIG. 3. Constant field, temperature-dependent sweeps of the in-plane resistance curves for single-crystal $HoNi_2B_2C$ for different values of the magnetic field applied along the c axis normalized to the value of resistance at 12 K in zero field, $R(T,H_a)/R(12\ \mathrm{K}, 0)$. The measuring current was 50 mA applied along the a axis which with sample dimensions (1.42 mm×0.52 mm×100 μm) gave a current density of 95 A/cm^2. Values of field in Oe are indicated by the numbers. Solid black arrows indicate a resistance anomaly at $T_1(H_a)$ associated with a first magnetic transition and an open arrow indicates a resistance anomaly at $T_N(H_a)$ associated with a second magnetic transition that coincides with the Néel temperature.

YNi_2B_2C material. The resistivity values of the two materials at low temperature are comparable, approximately 4 $\mu\Omega$ cm, but the resistivity ratio of the Y sample (16.5) is somewhat larger than for the Ho sample (11). Both samples show a large region where the temperature dependence is linear in T, typical of a good metal. In contrast, $TmNi_2B_2C$ single crystals (resistivity ratio 11.5) exhibit an almost linear dependence of resistivity on temperature right up to the superconducting transition at 10.5 K with practically no indication of saturation at a value of residual resistance.[23] At 300 K the values of $d\rho/dT$ are 0.22 and 0.15 $\mu\Omega$ cm/K for the Y and Ho samples, respectively. These are lower values of $d\rho/dT$ than reported in previous work.[7]

The normalized resistance with $I=50$ mA ($j=95$ A/cm^2) along the a axis as a function of temperature for different values of the magnetic field applied parallel to the c axis is illustrated in Fig. 3. For $H_a=0$, $T_c=8.7$ K (zero resistance), somewhat higher than the 8 K value reported for polycrystalline samples,[7] and there is no reentrance observed. As H_a increases, T_c decreases, and, by $H_a=50$ Oe (not shown in Fig. 3) a reentrant feature which grows with increasing field can be detected at 5.2 K. It is first shown for $R(T,H_a=100$ Oe) in Fig. 3. Besides the superconducting transition there are two other reproducible features associated with these data. The first is the dramatic loss of scattering in the normal state associated with the transition to the commensurate antiferromagnetic phase at 5.2 K, most clearly seen for $R(T,H_a=8.0$ kOe), an applied field at which the sample is fully normal. This feature corresponds to the lowest temperature magnetic transition in Fig. 1, T_N, and is indicated by the open arrow. For smaller fields, T_N is determined from the point of sharp discontinuity in slope of $R(T)$ just on the low-temperature side of the reentrant peak near 5.2 K. The second feature at about $T=6.0$ K (indicated by the solid black arrow for $H_a=900$ Oe, 1.5 kOe, 2 kOe, and 3.0 kOe) is associated with the highest temperature magnetic transition shown in Fig. 1, which in zero field corresponds to the onset of the spiral magnetic phase according to neutron scattering from single-crystal samples, and will be called T_1. Both T_1 and T_N determined from $R(T,H_a)$ are relatively field independent, consistent with the data in Fig. 1. We have thus established that not only does $R(T,H_a)$ indicate the superconducting T_c, but $R(T,H_a)$ also couples to two of the magnetic transitions and indicates their transition temperatures.

The normalized resistance with $I=50$ mA ($j=95$ A/cm^2) along the a axis as a function of different values of the magnetic field applied parallel to the b axis is illustrated in Fig. 4. For both Figs. 3 and 4 only data from a small percentage of the constant field sweeps actually measured are shown, and approximately half of the data points for each curve are shown. Again T_c is initially suppressed by increasing the applied field, and there is no reentrant behavior until $H_a=150$ Oe. For subsequent discussions we will define T_c by extrapolation of the steepest part of the superconducting transition to zero, but only if the resistance actually goes to zero in this temperature range. In the case of magnetic superconductors there is no theoretical description of $R(T)$ that can be used to precisely determine T_c, particularly near the reentrant region. Consequently, extrapolation to zero resistance is as good a choice as any. Features associated with both the upper magnetic transition T_1 (marked with solid black arrows for $H_a=1.3$ and 2.0 kOe) and the lower one T_N (marked with the open arrow for $H_a=4.0$ kOe) associated with the dramatic loss of scattering can be identified in Fig. 4(a). T_1 is relatively field independent and T_N, is suppressed with field, dropping from near 5.2 K at 250 Oe to near 4.5 K at 4.0 kOe. The field dependence of these two transitions are consistent with the preliminary data of Fig. 1. There is negligible hysteresis observed in the resistive transitions shown in either Fig. 3 or 4.

$R(T,H_a)$ for applied fields greater than the superconducting critical field at 2 K are shown in Fig. 4(b). These curves are offset for clarity since they actually cross between 2 and 4 K. For these curves, superconductivity and the transition to the commensurate antiferromagnet (that we associated with the large loss of scattering) are both completely suppressed

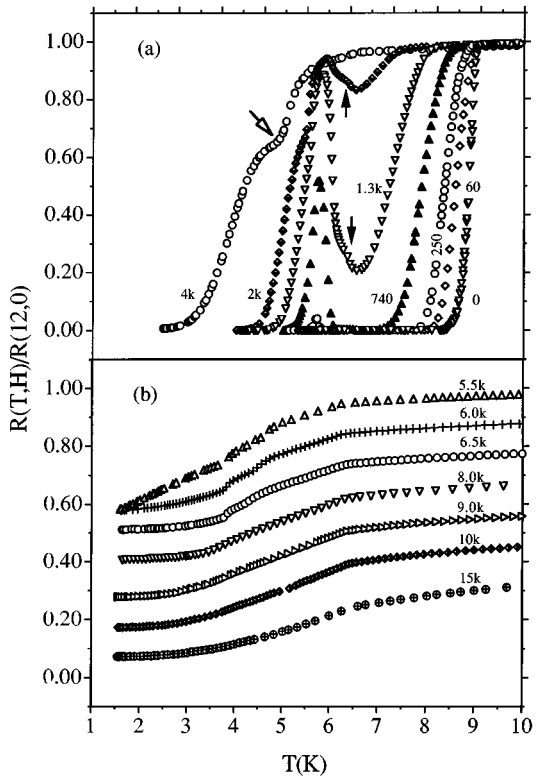

FIG. 4. Constant field, temperature-dependent sweeps of the in-plane resistance curves for different values of the magnetic field applied along the b axis normalized to the value of resistance at 12 K in zero field for the same single-crystal $HoNi_2B_2C$ sample and current as shown in Fig. 3. The arrows correspond to the same transitions indicated in Fig. 3; (a) values of the field in Oe are indicated by the numbers; (b) curves for H_a greater than the superconducting critical field such that the crystal is fully normal. The curves are shifted downward by 0.1 successively (i.e., the curve for 5.5 kOe is unshifted and that for 15 kOe is shifted down by 0.6) for clarity. Values of the field in Oe are indicated by the numbers.

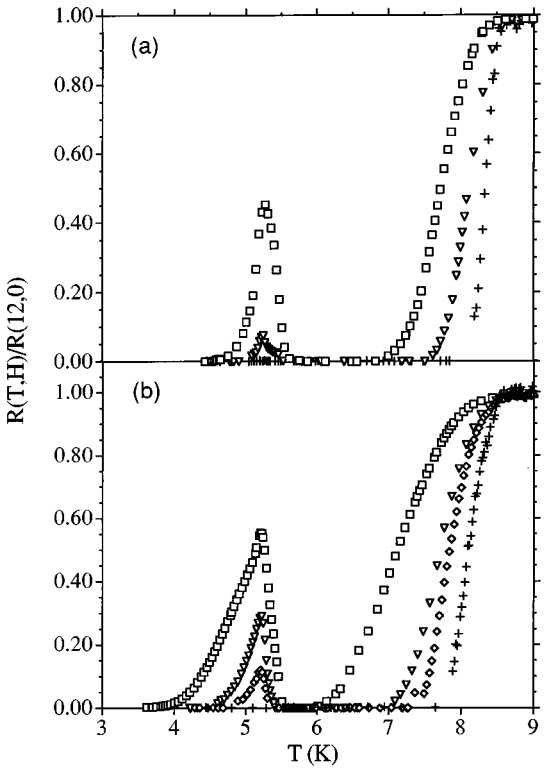

FIG. 5. (a) Normalized current dependence of $R(T, 650\ \text{Oe})$ with $\vec{H}_a$ along the b axis, **j** along the a axis: +, $j=1.9$ A/cm^2; ▽, $j=19$ A/cm^2; □, $j=95$ A/cm^2. (b) Normalized current dependence of R (T, 675 Oe) with with $\vec{H}_a$ along the c axis, $\vec{j}$ along the a axis: +, $j=1.9$ A/cm^2; ◇, $j=9.5$ A/cm^2; ▽, $j=19$ A/cm^2; □, $j=95$ A/cm^2.

over this range of field and temperature. We identify the break in slope near 6 K with the upper transition T_1 which appears to be still present even at 15 kOe. At about 3.8 K there appears to be a second break in slope for the curves with $H_a=5.5$, 6.0, 6.5, and 8.0 kOe. For higher fields this break is not clear, but rather a smooth continuous saturation of the resistance. These second features at T^* may represent a transition that has not previously been reported, but the evidence is inconclusive.

There is a current dependence observed for the resistance curves in the presence of a field for the Ho single crystals, but there is negligible current dependence in zero field or in the fully normal state, $H_a > H_{c2}(T=0)$, e.g., Fig. 4(b). Consequently, the current dependence is not a heating effect. Similarly we find negligible current dependence with or without a field for similar single-crystal Y samples and Tm samples[23] over the full temperature range covered by these measurements. Since those measurements were at similar current densities and resistances, a heating effect here would have also been observed for Y and Tm. We are aware of no previous reports of current dependences with polycrystalline samples of the superconducting quaternary borocarbides or earlier magnetic superconductors.

The effect of current on the resistive curves in a magnetic field is illustrated in Figs. 5(a) (H_a along the b axis) and 5(b) (H_a along the c axis). The field in Fig. 5(a) is 650 Oe while that in Fig. 5(b) is 675 Oe. A current increase broadens T_c and enhances the reentrant behavior. At the lowest current density shown (1.9 A/cm^2), the reentrant behavior can hardly be seen in these fields; whereas, at $j=95$ A/cm^2 it is prominent. Similar behavior was observed in the five other single-crystal samples studied, but the orientation of the current with respect to the crystal axes in the plane was not determined for these samples. It should be noted that the features identified with magnetic transitions in Figs. 3, 4, and 6 are not shifted by changes in the current, unlike the features associated with the superconducting transitions. Although there is a negligible current dependence of T_c observed for YNi_2B_2C and $TmNi_2B_2C$ single-crystal samples,[23] there appears to be a clearly observable current dependence in a field[24] for single-crystal $ErNi_2B_2C$ samples (but much smaller than for the $HoNi_2B_2C$ single crystals) grown by the same technique.

In order to more fully determine the superconducting and magnetic phase diagrams, $R(H)$ isotherms for several different temperatures have been measured as shown in Fig. 6. The solid circles show $R(H)$ for H_a parallel to the c axis at $T=4.35$ K. The sharp rise is associated with H_{c2} ($T=4.35$ K). Above this there are no other features, which is in accord

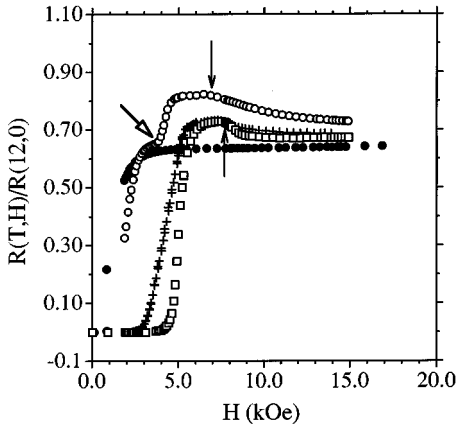

FIG. 6. Constant temperature field sweeps of the in-plane resistance normalized to the value at 12 K in zero field for the same $HoNi_2B_2C$ single crystal as shown in Figs. 3 and 4. For a field applied along the a axis □, $T=1.8$ K; +, $T=3.0$ K; ○, $T=4.35$ K; and for a field applied along the c direction ●, $T=4.35$ K. Current values and directions are the same as in Figs. 3 and 4. The open arrow corresponds to the feature designated by an open arrow in Fig. 4. The thin line arrows correspond to the transition at T_2 in Fig. 1(b).

with the sample remaining in the commensurate antiferromagnetic state to the highest measured fields. For the field applied along the $a(b)$ axis, the open circles ($T=4.35$ K) show an initial sharp rise associated with H_{c2}. Above this field $R(H)$ enters a plateau where the data follow closely that for H_a along the c axis at the same temperature. At a field of about $H_a=4$ kOe, there is a second sharp increase in resistance followed by a plateau and then a decrease in resistance. Below about 4 kOe we assume that the sample was in the commensurate antiferromagnetic state with a transition to the intermediate magnetic phase at this field, in good agreement with the data represented by solid symbols in Fig. 1. The sharp onset of negative magnetoresistance indicated by the thin black arrows represents the crossing of the second line of phase transitions corresponding to T_2 in the $d\chi T/dT$ data (solid symbols) of Fig. 1. The two curves at lower temperature provide data to extend this phase boundary, but the crossing of the commensurate antiferromagnetic boundary T_N for these two curves is obscured by the superconducting transition. It should be noted that the T_2 boundary has now saturated at about 8 kOe at these two lower temperatures, 1.8 and 3 K.

In order to separate H_{c2} and the lower magnetic transition T_N for the field applied along the a axis, a series of $M(H)$ isotherms were measured with the results shown in Fig. 7. Due to the large magnetic contribution from Ho^{3+} for this direction of applied field and the small values of H_{c1} ($H_{c1}\leqslant 300$ Oe for these temperatures), the magnetic response is virtually all due to that of the local moments. As shown below, these data also agree well with the $R(T,H)$ and earlier $M(T)$ data.[10,11]

DISCUSSION

Based on recent band-structure calculations[17,18] for the similar compound, $LuNi_2B_2C$, and the measurements reported here, estimates of the electron mean free path l, electron-phonon coupling constant λ, coherence length ξ_0, and the exchange integral I between the conduction electrons and the Ho^{3+} ions can be determined. Since the dominant states at the Fermi surface are Ni-3d states, the band Fermi velocity v_F and band density of states $N_b(0)$ for $HoNi_2B_2C$ are expected to be close to the values $v_F=3.6\times10^7$ cm/s (note that $v_F^2=v_{Fx}^2+v_{Fy}^2+v_{Fz}^2$ in Ref. 17) and $N_b(0)=4.8$ states/eV primitive unit cell calculated for $LuNi_2B_2C$. The electron mean free path can be estimated from the residual resistance $\rho_0=4$ μΩ cm at 10 K with the relation

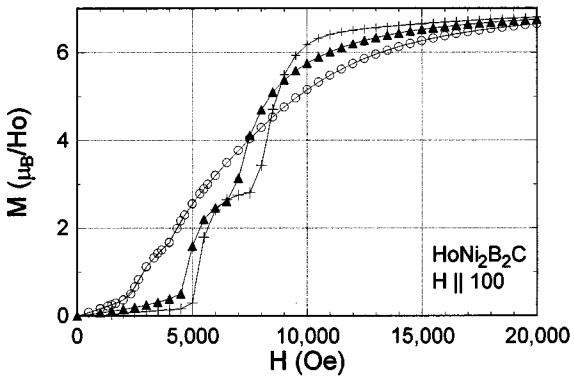

FIG. 7. Constant temperature sweeps of the magnetization $M(H_a)$ for magnetic field applied along the $a(b)$ axis for $HoNi_2B_2C$ single crystals: +, 2 K; ▲, 4 K; ○, 5 K.

$$\rho^{-1}=2e^2N(0)v_Fl/3 \tag{1}$$

which gives $l\approx 90$ Å. The coherence length ξ_0 can be estimated in the clean limit at $\xi_0=280$ Å from the relationship[25]

$$\xi_0=0.54[\phi_0/T_c(-dH_{c2}/dT)_{T=T_c}]^{1/2} \tag{2}$$

with $dH_{c2}/dT\approx 0.09$ T/K taken as a mean slope from Fig. 8(a) below for the low current measurements. In the dirty limit[25]

$$(\xi_0 l)^{1/2}=0.47[\phi_0/T_c(-dH_{c2}/dT)_{T=T_c}]^{1/2} \tag{3}$$

which gives $\xi_0=660$ Å with the same value for v_F. These estimates of ξ_0 may be compared to the value $\xi_0=\hbar v_F/\pi\Delta=580$ Å estimated using the band-structure value of v_F for $LuNi_2B_2C$ and the BCS value, $2\Delta=3.5k_B T_c$. With these values of ξ_0 and l the system appears to be neither in the clean limit nor in the dirty limit with $\xi_0/l\approx 2-8$.

In the Bloch-Grüneisen transport theory the temperature dependence of the resistivity can be related to the electron-phonon coupling λ_{tr} by the relation[17]

$$d\rho/dT=(8\pi^2/\hbar\Omega_P^2)k_B\lambda_{tr}, \tag{4}$$

where Ω_P is the Drude plasma frequency. For $LuNi_2B_2C$, the calculated value[17] of Ω_P is 5.1 eV. The use of this value for $HoNi_2B_2C$ with the value $d\rho/dT=0.15$ μΩ cm/K near room temperature gives $\lambda_{tr}=0.97$. For YNi_2B_2C $d\rho/dT$ is appreciably larger and $\lambda_{tr}=1.4$ with the same value for Ω_P. With the Debye temperature reported[26] for YNi_2B_2C ($\Theta_D=489$ K), application of Eq. (4) at room temperature is marginal; whereas, the Debye temperature for Ho is estimated to be much lower.[10]

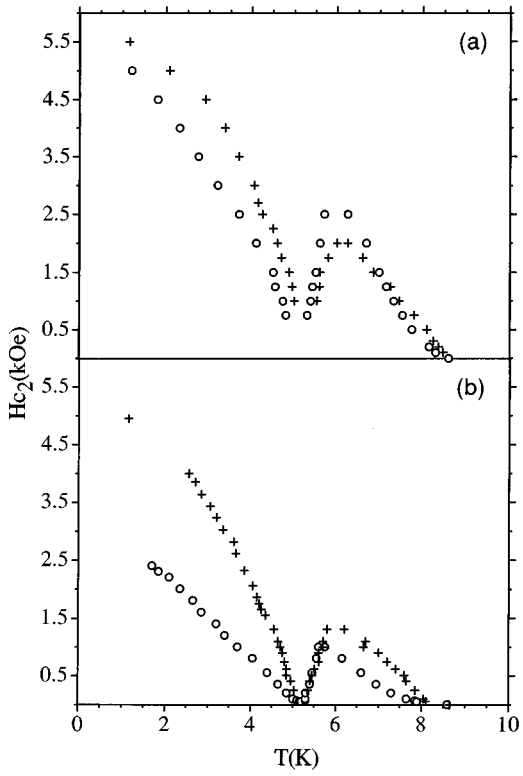

FIG. 8. Superconducting "phase diagram" $H_{c2}(T)$ for $HoNi_2B_2C$; (a) determined from resistance measurements with $\vec{H}_a$ applied along the b axis (crosses) and applied along the c axis (open circles) for low current, $j=1.9$ A/cm^2; (b) apparent superconducting "phase diagram" for higher current, $j=95$ A/cm^2. The symbols are the same as in (a). T_c is taken as the point at which the steepest part of the resistance curve extrapolates to zero resistance, but only if the sample resistance goes to zero in that region.

In the normal state, the resistivity of the sample can be expressed as the sum of the residual resistivity, that due to phonon scattering, and that from magnetic scattering by disordered spins, $\rho=\rho_0+\rho_p+\rho_{spd}$. The exchange constant I between the conduction electrons and the Ho^{3+} ions can be estimated from the contribution to the resistivity by spin disorder scattering ρ_{spd} according to the relation[27]

$$\rho_{spd}=\frac{3\pi N}{\hbar e^2 v_F^2} I^2(g-1)^2 J(J+1), \tag{5}$$

where N is the number of Ho atoms per unit volume, v_F the Fermi velocity, g the Landé g factor, and J the total angular momentum of the localized Ho ion in units of $\hbar$. Based on the abrupt drop in resistivity at T_N in Fig. 3, $\rho_{spd}\approx 1.6$ $\mu\Omega$ cm. With v_F calculated for $LuNi_2B_2C$, this gives the estimate $I=0.6$ eV Å^3.

Superconducting phase diagrams $[H_{c2}(T)]$ for $HoNi_2B_2C$ determined by resistance measurements for the applied field along the c axis and along the b axis are shown in Fig. 8(a) for $j=1.9$ A/cm^2 and in Fig. 8(b) for $j=95$ A/cm^2. Qualitatively, $H_{c2}(T)$ is similar for the low and higher current densities. $H_{c2}(T)$ increases from T_c to 6 K and then goes through a deep minimum at 5.2 K followed by an increase as temperature is lowered to 1.8 K. Quantitatively, $H_{c2}(T)$ is higher at all temperatures for the lower current density. Comparison between Figs. 8(a) and 8(b) shows the strong current dependence of the depth of the minimum in $H_{c2}(T)$ at 5.2 K and the anisotropy of the current dependence of $H_{c2}(T)$. This does not change dramatically if the midpoint of the resistive transition is chosen as T_c instead of the extrapolation of the steepest part to zero. The effect of the current is strongly dependent on the direction of the applied field as can be seen in the resistive curves in Figs. 5(a) and 5(b) as well as in the $H_{c2}(T)$ boundaries in Figs. 8(a) and 8(b). We emphasize again, that there is no current dependence in zero field. The current dependence, however, becomes obvious with the application of a field as small as 50 Oe. The anisotropy of the current dependence of the magnetoresistance (shown in Fig. 5) associated with the direction of the applied field is different from the anisotropy of the susceptibility, i.e., the current dependence is greater for H_a along the c axis while χ is greater in the ab plane, indicative of strong interplay between the superconductivity and magnetic ordering that can be strongly influenced by the currents. Neutron-scattering[12,13] and x-ray diffraction on comparable single crystals indicate a well-ordered crystal structure, and magnetization measurements on the same small sample used for resistance studies are in excellent agreement with those for much larger single-crystal samples previously[10,11] reported. There are, however, small lumps of flux residue on the crystals and perhaps small inclusions of flux in the crystals, but the residue flux material does not show a superconducting transition above 2 K.[24] Furthermore, we reiterate that there is negligible current dependence of $T_c(H)$ for similar single-crystal samples with $R=$Y and Tm,[23] which have similar residues of flux. On the other hand, there is a similar, but much weaker, current dependence for single-crystal samples with $R=$Er.[24] We speculate that the current dependence may be related to the ratio of the magnetic to the superconducting transition temperatures T_m/T_c which is 0.7, 0.6, 0.15, and 0 for $R=$Ho, Er, Tm, and Y, respectively, and occurs when this ratio is closer to unity.

If the current dependence were only observed in the region of temperature where neutron scattering indicates a modulated magnetic structure [from 5.2 to 6 K (Refs. 12 and 13) for single crystals, or to almost the zero field T_c (Refs. 14–16) for polycrystalline samples], one could argue that both superconductivity and magnetism might exhibit a modulated structure and that the spatially modulated superconductivity is very sensitive to the current density. The current dependence is, however, quite obvious, and also quite strong (particularly for H_a along the c axis), to temperatures well below the commensurate antiferromagnetic transition temperature T_N. In this commensurate magnetic phase with a wavelength equal to the lattice spacing, the superconducting order parameter should be uniform and unaffected by the magnetic order, and no modulated structure was seen below 5 K for single crystals.[12,13] A similar current dependence has not been reported for polycrystalline samples.[7,28,29] Another important difference between these single-crystal measurements and previous results from polycrystalline samples[7] is that for current densities up to 95 A/cm^2, the superconductivity in the single crystals is not reentrant in zero field. (More recent measurements for polycrystalline samples[28,29] do not appear to show reentrance in zero field, indicating a

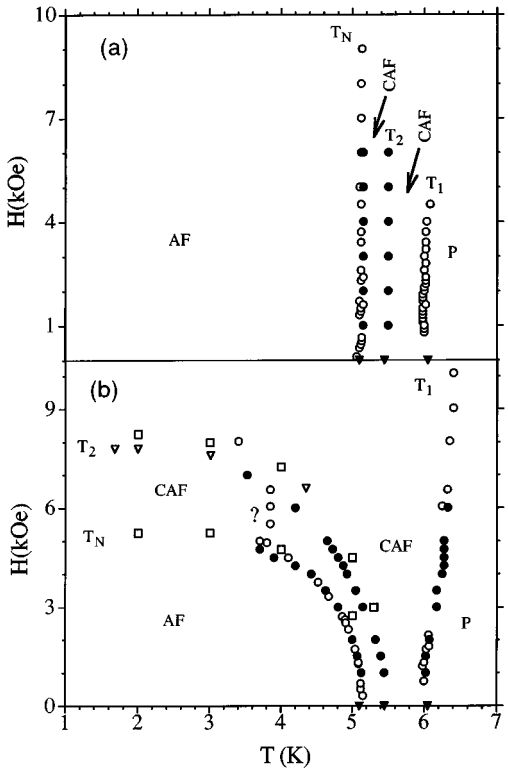

FIG. 9. Magnetic "phase diagram" for $HoNi_2B_2C$, (a) H_a along the c axis; (b) H_a along the $a(b)$ axis from a wide range of measurements: ▼, $C_p(H_a=0)$, Ref. 10; ●, $d\chi T/dT$, Refs. 10 and 11; ▽, $R(H)$; ○, $R(T)$; □, $M(H)$ this work.

sample to sample variation in polycrystalline samples.) A field of at least 50 Oe, greater for H_a in the ab plane, must be applied to see reentrant behavior with this current density, and the minimum field increases with decreasing current. The absence of zero-field reentrant behavior is consistent with both magnetism measurements for comparable $HoNi_2B_2C$ samples[10] and the behavior of previously discovered antiferromagnetic superconductors.[30]

The magnetic phase diagrams based on five different sets of data: $C_p(H=0)$,[10] $d\chi T/dT$,[10,11] $M(H)$ isotherms, $R(H)$ isotherms, and $R(T)$ at constant applied field (the last three from results presented here) are shown in Figs. 9(a) and 9(b). For clarity, only a few data points from $d\chi T/dT$ and $R(T)$ are shown in Fig. 9. The agreement between thermodynamic and transport measurements on at least six different crystals from different batches of flux grown crystals is truly remarkable and convincing. The phase diagrams show a rich variety of magnetic phases. For H_a along the c axis there are three magnetically ordered phases, the commensurate antiferromagnetic (AF) phase below about 5 K and two complex antiferromagnetic (CAF) phases between about 5 and 6 K. These phases appear to be robust to quite large fields. For H_a along the $a(b)$ axis there are at least three distinct ordered magnetic phases, perhaps a fourth based on T^* discussed with $R(T)$ data from Fig. 4(b), whose boundary (vertical region near 3.8 K) in Fig. 9(b) is marked with a question mark. The question mark indicates that we do not have thermodynamic (M or $d\chi T/dT$) data in this region that can confirm this boundary as in the case for the other three boundaries. The phases include the commensurate

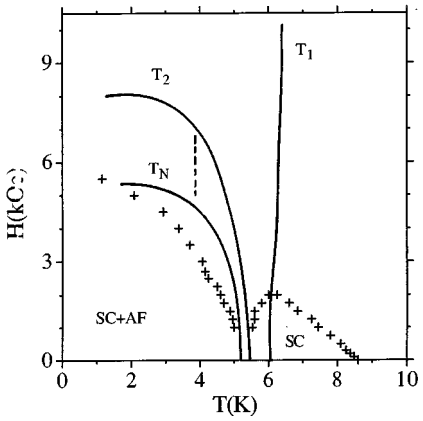

FIG. 10. Combined phase diagram, $H_{c2}(T)$ and magnetic phase boundaries for H_a along the $a(b)$ axis. $H_{c2}(T)$ (represented by crosses) is taken from the low current ($j=1.9$ A/cm^2) data in Fig. 8(a) and the lines for the magnetic boundaries represent the data from Fig. 9(a). The dashed line represents the possible vertical boundary marked with a question mark in Fig. 9(b) and discussed in the text.

antiferromagnetic phase and two complex antiferromagnetic phases. The first of these, delineated by the temperatures $T_1(H)$, appears to be robust up to at least 15 kOe. On-going analysis of single-crystal neutron-diffraction data taken with H_a parallel to the $a(b)$ axis should soon provide further identification of these two complex antiferromagnetic phases.[31]

Figure 10 summarizes the results for H_a along the $a(b)$ axis with $H_{c2}(T)$ (crosses) taken from the low current data in Fig. 8(a) and the lines for the magnetic phase boundaries representing the data from Fig. 9(b). Below 8 K, $H_{c2}(T)$ rises linearly with temperature to 6 K where it crosses the line $T_1(H_a)$, the boundary for the first CAF phase. It then drops abruptly to a minimum located between the lines $T_2(H_a)$ and $T_N(H_a)$, the boundaries for the second CAF phase and the commensurate AF phase. Below $T_N(H_a)$ it begins to rise sharply again, in the AF phase. These data are consistent with either or both of the CAF phases being detrimental to superconductivity. Between 6 and 5 K the presence of longer wavelength a^* and c^* periodicity has been observed in the neutron scattering data[12,13] which would be expected to suppress superconductivity. It is, however, not yet clear from neutron scattering what change in ordering occurs on crossing $T_2(H_a)$. Significant deviations between $H_{c2}(T)$ and $T_N(H_a)$ in the 3–5 K range are obvious in this figure. At lower temperatures (near 2 K) $H_{c2}(T)$ approaches $T_N(H_a)$. This behavior indicates that superconductivity is not necessary for stabilization of the antiferromagnetic phase. This is also obvious upon comparing $H_{c2}(T)$ with $T_N(H_a)$ for the field applied along the c axis where $T_N(H_a)$ is practically independent of field while $H_{c2}(T)$ shows appreciable curvature.

CONCLUSIONS

Rich detail has been observed in the resistive transitions in magnetic fields of single-crystal $HoNi_2B_2C$. For the single-crystal samples, no reentrant superconductivity was observed in zero field. An unusual current dependence of the

superconducting transition is observed that has not been reported for polycrystalline $HoNi_2B_2C$ samples or other magnetic superconductors. It is not clear if this current dependence is due to the existence of a spiral magnetic phase. Since it is negligible for single crystals with R=Y, Tm (Ref. 23) and much weaker for R=Er,[24] the ratio of T_m to T_c may play a role. Low-temperature scanning force microscopy studies of the intermediate state for single crystals could be helpful in identifying magnetic structures that might indicate the mechanism of interplay between the superconductivity and magnetism as a function of biasing current in this region of the phase diagram. Three features (current independent) that can be identified with magnetic phases have been observed in the resistance curves. Exceptional agreement between five different types of measurements on more than six different single crystals flux grown from different batches provides a detailed, definitive phase diagram for $HoNi_2B_2C$. The complexity and anisotropy of the phase diagram in this system attests to the necessity for single-crystal samples when interpreting measurements in a nonzero magnetic field. These materials are neither ''clean'' nor ''dirty'' superconductors with $\xi_0 \approx 600$ Å, $l \approx 90$ Å, and exchange parameter, $I \sim 0.6$ eV Å^3.

ACKNOWLEDGMENTS

Work at Texas A&M University was supported by the Robert A. Welch Foundation (Grant No. A-0514). Ames Laboratory was operated for the U. S. Department of Energy by Iowa State University under Contract No. W-7405-ENG-82. The work at Ames was supported by the Director for Energy Research, the Office of Basic Energy Sciences. We wish to thank T. Hughbanks for determination of the $HoNi_2B_2C$ single-crystal orientation. Two of us (K.D.D.R. and D.G.N.) acknowledge helpful discussions with L. N. Bulaevskii, C. R. Hu, and V. Pokrovsky.

[1] R. Nagarajan, C. Mazumdar, Z. Hossain, S. K. Dhar, K. V. Gopalakrishnan, L. C. Gupta, C. Godart, B. D. Padalia, and R. Vijayaraghavan, Phys. Rev. Lett. **72**, 274 (1994).

[2] R. J. Cava, H. Takagi, B. Batlogg, H. W. Zandbergen, J. J. Krajewski, W. F. Peck, Jr., R. B. van Dover, R. J. Felder, T. Siegrist, K. Mizuhashi, J. O. Lee, H. Eisaki, S. A. Carter, and S. Uchida, Nature **367**, 146 (1994).

[3] T. Siegrist, H. W. Zandbergen, R. J. Cava, J. J. Krajewski, and W. F. Peck, Jr., Nature **367**, 254 (1994).

[4] R. J. Cava, H. Takagi, H. W. Zandbergen, J. J. Krajewski, W. F. Peck, Jr., T. Siegrist, B. Batlogg, R. B. van Dover, R. J. Felder, K. Mizuhashi, J. O. Lee, H. Eisaki, and S. Uchida, Nature **367**, 252 (1994).

[5] B. K. Cho, P. C. Canfield, and D. C. Johnston, Phys. Rev. B **52**, 3844 (1995).

[6] P. Dervenagas, J. Zarestky, C. Stassis, A. I. Goldman, P. C. Canfield, and B. K. Cho, Physica, B **212**, 1 (1995).

[7] H. Eisaki, H. Takagi, R. J. Cava, B. Batlogg, J. J. Krajewski, W. F. Peck, Jr., K. Mizuhashi, J. O. Lee, and S. Uchida, Phys. Rev. B **50**, 647 (1994).

[8] B. K. Cho, M. Xu, P. C. Canfield, L. L. Miller, and D. C. Johnston, Phys. Rev. B **52**, 3676 (1995).

[9] B. K. Cho, P. C. Canfield, L. L. Miller, D. C. Johnston, W. P. Beyermann, and A. Yatskar, Phys. Rev. B **52**, 3684 (1995).

[10] P. C. Canfield, B. K. Cho, D. C. Johnston, D. K. Finnemore, and M. F. Hundley, Physica C **230**, 397 (1994).

[11] P. C. Canfield, B. K. Cho, D. C. Johnston, and M. F. Hundley, in *Neutron Scattering in Materials Science II*, edited by D. A. Neumann, T. P. Russell, and B. J. Wuensch, MRS Symposia Proceedings No. 376 (Materials Research Society, Pittsburgh, 1995).

[12] A. I. Goldman, C. Stassis, P. C. Canfield, J. Zarestky, P. Dervenagas, B. K. Cho, D. C. Johnston, and B. Sternlieb, Phys. Rev. B **50**, 9668 (1994).

[13] C. Stassis, A. I. Goldman, P. Dervenagas, J. Zarestky, P. C. Canfield, B. K. Cho, D. C. Johnston, and B. Sternlieb, in *Neutron Scattering in Materials Science II* (Ref. 11).

[14] T. E. Grigereit, J. W. Lynn, Q. Huang, A. Santoro, R. J. Cava, J. J. Krajewski, and W. F. Peck, Jr., Phys. Rev. Lett. **73**, 2756 (1994).

[15] Q. Huang, A. Santoro, T. E. Grigereit, J. W. Lynn, R. J. Cava, J. J. Krajewski, and W. F. Peck, Jr., Phys. Rev. B **51**, 3701 (1995).

[16] C. V. Tomy, L. J. Chang, D. McK. Paul, N. H. Andersen, and M. Yethiraj (unpublished).

[17] W. E. Pickett and D. J. Singh, Phys. Rev. Lett. **72**, 3702 (1994).

[18] L. F. Mattheiss, Phys. Rev. B **49**, 13279 (1994).

[19] Ø. Fischer, in *Ferromagnetic Materials*, edited by K. H. J. Buschow and E. P. Wohlfarth (North-Holland, Amsterdam, 1990), pp. 465–548.

[20] L. N. Bulaevskii, A. I. Buzdin, M. L. Kulić, and S. V. Panjukov, Adv. Phys. **34**, 175 (1985).

[21] M. Xu, P. C. Canfield, J. E. Ostenson, D. K. Finnemore, B. K. Cho, Z. R. Wang, and D. C. Johnston, Physica C **227**, 321 (1994).

[22] B. K. Cho, B. N. Harmon, D. C. Johnston, and P. C. Canfield, Phys. Rev. B **53**, 2217 (1996).

[23] K. D. D. Rathnayaka, D. G. Naugle, B. K. Cho, and P. C. Canfield (unpublshed).

[24] P. C. Canfield (private communication).

[25] P. G. de Gennes, *Superconductivity of Metals and Alloys* (W. A. Benjamin, New York, 1966).

[26] R. Movshovich, M. F. Hundley, J. D. Thompson, P. C. Canfield, B. K. Cho, and A. V. Chubukov, Physica C **227**, 381 (1994).

[27] E. Gratz and M. Zuckermann, in *Handbook on the Physics and Chemistry of Rare Earths*, edited by K. A. Geschneider, Jr. and L. Eyring (North-Holland, Amsterdam, 1982), p. 138.

[28] S. A. Carter, B. Batlogg, R. J. Cava, J. J. Krojewski, and W. F. Peck, Jr., Phys. Rev. B **51**, 12 644 (1995).

[29] M. S. Lin, J. H. Shich, Y. B. You, W. Y. Guan, H. C. Ku, H. D. Yang, and J. C. Ho, Phys. Rev. B **52**, 1181 (1995).

[30] M. B. Maple, in *Advances in Superconductivity*, edited by B. Deaver and J. Ruvalds (Plenum, New York, 1982), pp. 279–346.

[31] A. I. Goldman (private communication).